frontiers | Frontiers in Energy Research

TYPE Original Research
PUBLISHED 30 October 2023
DOI 10.3389/fenrg.2023.1303522



OPEN ACCESS

EDITED BY
Zhengmao Li,
Aalto University, Finland

REVIEWED BY
Xiaozhen Zhao,
Hebei University of Technology, China
Yan Zhang,
Liaoning University of Technology, China

*CORRESPONDENCE
Haoyu Chen,
237007432@qq.com
Zhenhua Li,
lizhenhua1993@163.com

RECEIVED 28 September 2023
ACCEPTED 12 October 2023
PUBLISHED 30 October 2023

CITATION
Chen H, Cheng J, Li Z, Abu-Siada A and Li H (2023), Distributed photovoltaic power fluctuation flattening strategy based on hybrid energy storage. *Front. Energy Res.* 11:1303522. doi: 10.3389/fenrg.2023.1303522



# Distributed photovoltaic power fluctuation flattening strategy based on hybrid energy storage

Haoyu Chen[1]*, Jiangzhou Cheng[1], Zhenhua Li[1]*, A. Abu-Siada[2] and Hongbin Li[3]

[1]College of Electrical Engineering and New Energy, Three Gorges University, Yichang, China, [2]Department of Electrical and Computer Engineering, Curtin University, Perth, WA, Australia, [3]State Key Laboratory of Advanced Electromagnetic Engineering and Technology, Wuhan, China

Aiming at mitigating the fluctuation of distributed photovoltaic power generation, a segmented compensation strategy based on the improved seagull algorithm is proposed in this paper. In this regard, a hybrid energy storage system comprising a lithium battery and supercapacitor is utilized. The internal power distribution of the hybrid energy storage system is adjusted using wavelet packet decomposition, and the state of charge is employed to adapt the primary power distribution. The start and end times for charging and discharging are determined by combining the time of use, electricity price, state-of-charge information, and load size at night to realize the economic operation of the system. The opposing search operator strategy and mutation operation are used to improve the seagull algorithm, optimize the controller parameters of the DC/DC converter, and improve its response time. Combined with the historical measured data of a distributed photovoltaic in Hubei Province, simulation results show that the proposed strategy can effectively smoothen the fluctuation of distributed photovoltaic generated power while reducing the charging and discharging frequencies of the energy storage system, hence improving its stability and service life.

KEYWORDS

**distributed photovoltaic, power fluctuation, hybrid energy storage, segmentation compensation policy, seagull algorithm**

## 1 Introduction

Owing to its clean and relatively cheap energy, distributed photovoltaic technology is undergoing rapid development. However, due to the intermittency of solar irradiance, power generation of distributed photovoltaics is subjected to fluctuations, which seriously affects the reliability and stability of the entire grid (Pinheiro et al., 2021; Yang et al., 2022a). Therefore, smoothing out the fluctuation of the generated power of large-scale distributed photovoltaic systems has become a research hotspot.

The two-quadrant operational mode of the energy storage system plays a vital role in smoothing power fluctuations (Kawabe and Nanahara, 2018; Yang et al., 2022b; Zhang et al., 2022). Li et al. (2021a), Shi et al. (2021), Li et al. (2022), and Li et al. (2023a) use batteries to achieve power stabilization and employ economic evaluation indicators to improve the comprehensive economic strategy of the system. Choi et al. (2018) present a strategy based on load forecasting and energy storage for a rapid smoothing of power fluctuations. However, only one energy storage device (battery) has been utilized, which results in frequent charging and discharging that seriously affects the service life of the battery. Chen et al. (2022) and Xu et al. (2023) adopt a hierarchical compensation strategy for hybrid energy

storage systems to effectively compensate for power fluctuations. Ming et al. (2018), Li et al. (2021b), and Li et al. (2021c) use adaptive wavelet packet variation to optimize the hybrid energy storage charge and discharge powers. Xie et al. (2015) propose a quantum behavior particle optimization algorithm to optimize the energy storage configuration capacity and improve the power fluctuation compensation ability. In the aforementioned literature, hybrid energy storage devices are used to smooth out power fluctuations, but there are some concerns over the safety and economy of the used energy storage devices.

Regarding controller optimization, Nan et al. (2018) and Kharrazi et al. (2020) use the moth firefighting algorithm to optimize the parameters of the proportional–integral (PI) controller of the dynamic voltage restorer to achieve rapid recovery of voltage fluctuations. Izci et al. (2022), Fu et al. (2023), and Zhang et al. (2023) use the particle swarm algorithm to optimize the design of the controller parameters and to overcome the issue of large energy consumption of controller data debugging. You et al. (2022) introduce an adaptive weight balancing strategy into the seagull optimization algorithm to realize proportional–integral–derivative (PID) parameter optimization and improve controller performance. Maneesh (2015), Hao et al. (2022), and Li et al. (2023b) use SISO feedback technology to tune the PI controller parameters. The aforementioned literature reveals that the seagull optimization algorithm encompasses a wide search range and good robustness in optimizing controller parameters. The study by Yang et al. (2021a) is the first to use the SCUC expert system based on expanded sequence to sequence (E-Seq2Seq) to dynamically adjust the input parameters for optimal control of the controller. In addition, it can adapt and optimize the controller parameters rapidly according to the actual situation. However, it is still prone to problems, such as immature convergence and inability, to obtain a global optimal solution.

To overcome the aforementioned limitations on the existing literature, this paper proposes a hybrid energy storage system comprising a battery and supercapacitor connected to the DC bus of a distributed photovoltaic system through a DC/DC converter. A segmented compensation control strategy is employed to smoothen the generated power of the distributed photovoltaic system based on the system operating condition and power fluctuation. The state-of-charge (*SOC*) information is used to adjust the power, reduce the frequency of battery charging and discharging, and extend the service life of the energy storage system. Combined with time-of-use electricity price, state-of-charge information, and load size, the electricity price difference is used to determine the energy storage start and end times of charging and discharging. The seagull algorithm is improved by adopting an opposing search operator strategy and mutation operation to correct and tune the DC/DC converter controller parameters in order to improve its response speed and accuracy. Historical measured data of a distributed photovoltaic system in Hubei, China, are used to validate the robustness and feasibility of the proposed strategy.

## 2 Photo-storage collaborative operation system

The cooperative operation structure of the distributed photovoltaic and hybrid energy storage system is shown in Figure 1. The figure contains a distributed photovoltaic (PV) system, various types of loads, conventional power supply, and an AC bus. The hybrid energy storage system is connected to the DC bus through the converter (Zhu et al., 2022). The coordinated control system monitors the distributed photovoltaic output power in real time.

The specific working principle of the photo-storage joint operation system is explained as follows.

During daytime, distributed photovoltaics are mainly used to supply power to the loads, and the power balance equation during the transient process can be expressed as follows:

$$CU_{dc}\frac{dU_{dc}}{dt} = P_{pv} - P_{load} \pm P_{Bess}, \tag{1}$$

where $C$ is the DC terminal capacitance of the inverter, $U_{dc}$ is the DC terminal voltage of the inverter, $P_{Bess}$ is the power of the hybrid energy storage device that could be absorbed or released, and $P_{pv}$ and $P_{load}$ are, respectively, the PV and load power.

When the load power is certain and the output power of the distributed photovoltaics is affected by external factors, the power absorbed or released by the hybrid energy storage device confirms the power balance of the system according to Eq. 1. The hybrid energy storage device combines the characteristics of high energy density of the battery to smooth the low-frequency power fluctuation and the fast response and high number of charge and discharge times to smooth the high-frequency power fluctuation.

During nighttime, the conventional power supply is mainly used to supply power to the loads, whereas the hybrid energy storage device discharges its stored energy during the peak periods of electricity consumption and charges during the trough period according to the remaining capacity of the battery.

## 3 Hybrid energy storage control strategy

In order to reduce the fluctuation of distributed photovoltaic output power, ensure stable system operation, and extend the practical life of the battery, a segmented compensation control strategy for the hybrid energy storage system, as shown in Figure 2, is proposed.

First, the data acquisition center in the coordinated control system collects the distributed photovoltaic output power ($P_{pv}$) in real time, the power required for the load ($P_{load}$), and the conventional power supply ($P_{total}$). This study followed the measurement method described in Li et al. (2020), and the working state of the hybrid energy storage device is judged and divided into operating and latching states. When the system determines an operating state for the hybrid energy storage system, the output power of the battery and the supercapacitor is initially distributed. Then, the working state of the hybrid energy storage system is reassessed through the state-of-charge information fed back by the battery management system (BMS). If it is still in operation, the power protection unit limits the output power of the battery and supercapacitor branch using the state-of-charge information and updates the corresponding reference values for batteries and supercapacitors ($P_{batref}, P_{capref}$). The power of the hybrid storage system is then redistributed to obtain the final output power value ($P_{bat}, P_{cap}$).

The wavelet packet decomposition algorithm has good robustness and stability for high- and low-frequency signal

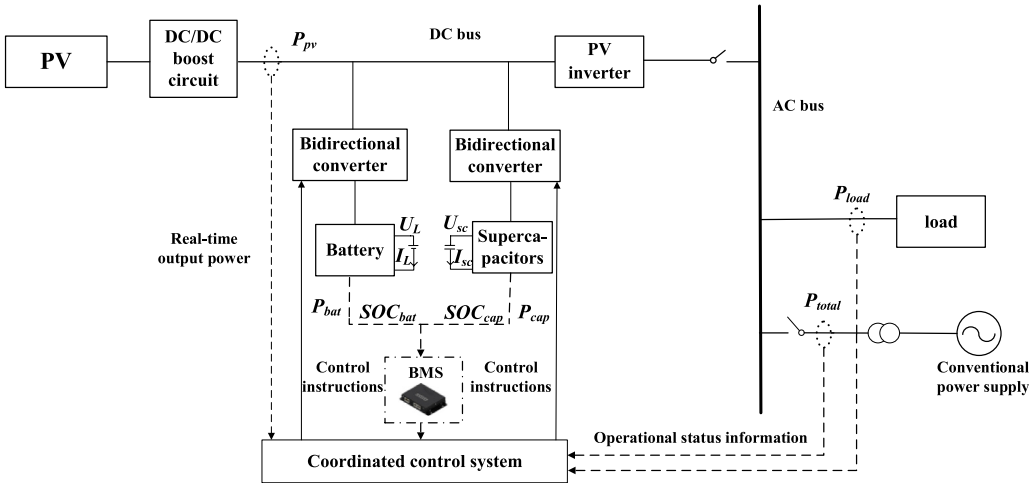


FIGURE 1
Structure diagram of the photo-storage collaborative operation system.

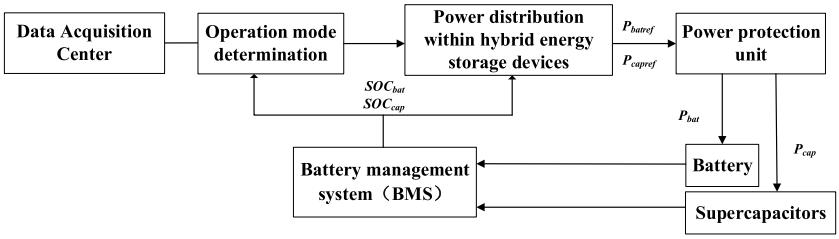


FIGURE 2
Control principle of the hybrid energy storage system.

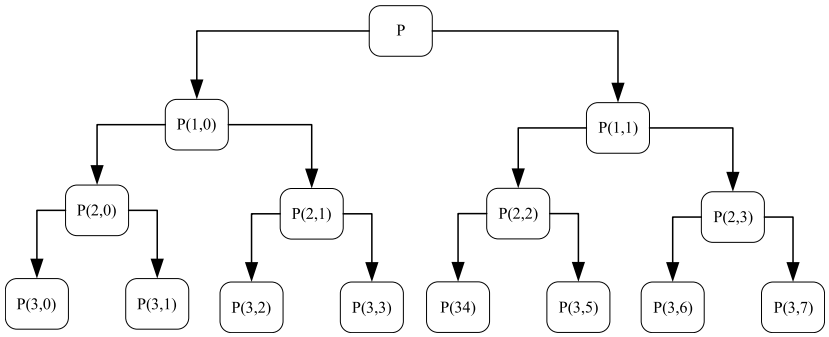


FIGURE 3
Schematic diagram of wavelet packet decomposition.

decomposition. The concept and calculation process of the wavelet packet algorithm are described in Weng et al. (2023). In this paper, the db6 wavelet packet algorithm is used to decompose the n-layer output power of a 750 kW distributed photovoltaic system installed in Hubei Province, China. After reconstructing the decomposition results, the output power signals ($P_i$) of $2^n$ different frequency bands are obtained, as shown in the schematic diagram in Figure 3. Based on the response time range of the battery and supercapacitor, a response frequency of $1.81 \times 10^{-2}$ Hz at a time scale of 1 min is used as its decomposition frequency. The first frequency band signal meets the distributed photovoltaic grid-connected power change standard and is used as the grid-connected reference power signal

**TABLE 1 PV grid-connected power change standards.**

| Type of PV | Output power variation/kW | |
|---|---|---|
| | Time scale 10 min | Time scale 1 min |
| Small scale | Installed capacity | Installed capacity/5 |
| Medium scale | Installed capacity | Installed capacity/5 |
| Large scale | Installed capacity/3 | Installed capacity/10 |

($P_{grid}$). The distributed photovoltaic grid-connected standards according to the literature (Technical regulations for connecting photovoltaic power stations to the power grid, 2011) are listed in Table 1.

The hybrid energy storage device initially allocates the remaining power required to stabilize the system. The $P_2 \sim P_5$ low-band power component is similar to the battery discharge frequency and is borne by the battery, while the remaining frequency bands are borne by the supercapacitor. The initial power distribution within the hybrid energy storage system can be represented using Eq. 2. The battery is charged at $P_{\text{batref}1} > 0$, and the supercapacitor is charged at $P_{capref1} > 0$ and *vice versa*.

$$\begin{cases} P_{grid} = P_1, \\ P_{batref1} = P_2 + P_3 + .... + P_5, \\ P_{capref1} = P_6 + P_7 + .... + P_m, \end{cases} \tag{2}$$

where $P_{batref1}$ is the reference value of the initial power allocation of the battery and $P_{capref1}$ is the initial power allocation reference value of the supercapacitors.

The aforementioned method considers the flattening effect of the power fluctuations in the process of power distribution. However, the supercapacitor and battery *SOC* modes are constantly changing during the flattening process, so *SOC* needs to be introduced as a constraint to correct the initial power distribution and reduce the phenomenon of overcharge and over-discharge.

Battery and supercapacitor *SOC* modes can be represented as (Zhang et al., 2022)

$$\begin{cases} P_{\text{BESS}}(t) = P_{\text{BESS}}(t-1) + \int \Delta P_t \times \Delta t, \\ SOC(t) = SOC(t-1) + \dfrac{\int \Delta P_t \times \Delta t}{P_{\text{BESS}}}, \end{cases} \tag{3}$$

where $\Delta P$ is the amount of power change.

In order to avoid frequent charging and discharging of the energy storage during the stabilization of power fluctuations, *SOC* should fluctuate between 30% and 80% (Shi et al., 2021) to ensure that the energy storage system has enough electric energy for charging and discharging. The references and Eq. 3 are combined to divide the *SOC* modes of the energy storage system. The threshold overcharge warning line value ($SOC_{high}$) is set to 0.8, and the corresponding battery and supercapacitor overcharge warning reference powers $P^*_{bath}(t)$ and $P^*_{bath}(t)$ are obtained. The threshold over-discharge warning line value ($SOC_{low}$) is set to 0.3, and the corresponding battery and supercapacitor over-discharge warning reference powers $P^*_{batl}(t)$ and $P^*_{\text{capl}}(t)$ are obtained. Hence, the *SOC* modes of the energy storage system include the overcharge warning area (0.8 ~ 1), normal working area (0.3 ~ 0.7), and over-discharge warning area (0 ~ 0.3).

When the *SOC* is within the normal operating area, the reference power assigned to the initial power does not need to be corrected. On the other hand, when the *SOC* is in the warning area, the reference power allocated by the initial power needs to be corrected accordingly. If the *SOC* works in the overcharge warning area, the next moment $P_{batref1}$ and $P_{capref1}$ are judged, and the reference power $P_{\text{batref}1} > 0$ or $P_{capref1} > 0$ is discharged without control. On the contrary, when the reference power is $P_{\text{batref}} < 0$ or $P_{capref} < 0$, it is necessary to delay the charging speed and adjust the output power. The principle of *SOC* working in the over-discharge warning area is similar to the aforementioned process, and the output power is corrected according to Eqs 4, 5, and the charge and discharge operational modes are stopped when *SOC* = 0.9 and *SOC* = 0.2, respectively.

$$\begin{cases} P_{bat}(t) = \dfrac{0.9 - SOC_t}{0.9 - SOC_{\text{high}}} P_{batref1}(t), \\ P_{cap}(t) = \dfrac{0.9 - SOC_t}{0.9 - SOC_{high}} P_{capref1}(t), \end{cases} \tag{4}$$

$$\begin{cases} P_{bat}(t) = \dfrac{SOC_t - 0.2}{SOC_{low} - 0.2} P_{batref1}(t), \\ P_{cap}(t) = \dfrac{SOC_t - 0.2}{SOC_{low} - 0.2} P_{capref1}(t), \end{cases} \tag{5}$$

where $SOC_r$ is the state of charge of the battery at moment t; $P_{bat}$ is the actual output power of the battery after the second correction of power, and $P_{cap}$ is the actual output power of the supercapacitor after the second correction of power.

From the perspective of system operation economy, the hybrid energy storage system combines time-of-use electricity prices at night and at peak periods, and part of the load demand is borne by the battery. At the valley electricity price, the hybrid energy storage device is charged through the conventional power supply. The control system combines information such as load size to determine the operating status of the hybrid energy storage device and the rules, which can be represented using Eq. 6.

$$\begin{cases} \text{Peak load periods:} \\ \begin{cases} \begin{cases} P_{load}(t) \geq P_{high}(i) \\ SOC(t) > SOC_{Low} \end{cases} \rightarrow \text{Energy storage device discharge} \\ \begin{cases} P_{load}(t) \leq P_{high}(i) \\ SOC(t) < SOC_{Low} \end{cases} \rightarrow \text{Energy storage shutdown} \end{cases} \\ \text{Low load peak periods:} \\ \begin{cases} \begin{cases} P_{load}(t) \leq P_{low}(i) \\ SOC(t) < SOC_{Low} \end{cases} \rightarrow \text{Energy storage device charging} \\ \begin{cases} P_{load}(t) \leq P_{low}(i) \\ SOC(t) > SOC_{Low} \end{cases} \rightarrow \text{Energy storage shutdown} \end{cases} \end{cases} \tag{6}$$

where $P_{high}(i)$ and $P_{low}(i)$ are the load thresholds during the peak-to-valley period of the electricity price and i represents the peak–valley time.

During peak power consumption periods, the load demand exceeds the set threshold, and when the *SOC* of the hybrid energy storage device is higher than the minimum set value, the device is discharged; otherwise, it is stopped. Similarly, during low power consumption periods, the load demand is lower than the set threshold, and when the *SOC* of the hybrid energy storage device is lower than the maximum set value, the device is charged; otherwise, it is shut down and held in a locked state.

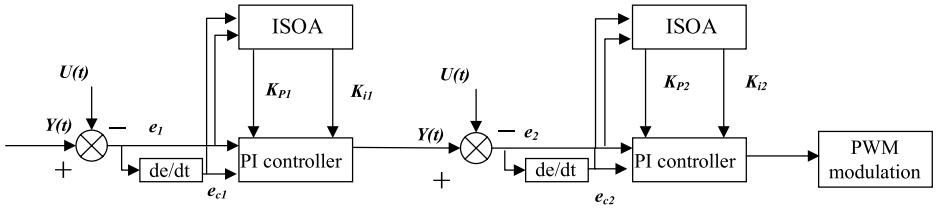


FIGURE 4
Schematic of controller optimization.

# 4 Optimum PI control parameters

In view of the disadvantages of the seagull optimization algorithm (SOA) described in *Introduction*, this paper introduces opposing search operators and mutation operations to improve the traditional SOA, as elaborated in the following paragraphs.

SOA is similar to other population optimization algorithms. Because the specific position of the optimal solution is uncertain and the initial population is initialized in a random way, the opposing search operator strategy is introduced into SOA.

The opposing search operator is used to optimize the initial population to produce the current and the opposing individuals ($x_i$, $\bar{x}$) within the interval $[L, U]$, which can be represented using Eq. 7.

$$\bar{x} = L + U - x_i. \tag{7}$$

According to the aforementioned definition, the following initialization method is used to update the current individual: set the population size N, compare the current and opposing individuals, and obtain the individual with the best fitness value, which is used as the initial population. The final initialization formula can be represented as

$$x_i = \begin{cases} \bar{x} f(\bar{x}) < f(x_i), \\ x_i, \end{cases} \tag{8}$$

where $x_i$ is the current individual and $\bar{x}$ is the individual opposite of the current individual.

In order to realize the online adjustment and tuning of controller parameters, the individual seagull is mutated as described in the following paragraph.

With a probability of 1/d, a certain element $x_j = (x_{j1}, x_{j2}...x_{jd})$ is randomly selected from the seagull individual $x_k\,(k = 1, 2, 3...d)$, and random numbers are generated in the lower and upper bound uj range instead of the elements in the seagull individual xj. Finally, a new individual $\overrightarrow{x_j} = (\overrightarrow{x_{j1}}, \overrightarrow{x_{j2}}...\overrightarrow{x_{jd}})$ is generated.

The variability operation formula can be represented as

$$x_j^{'} = \begin{cases} l_j + \lambda\left(u_j - l_j\right), j = k, \\ x_j, otherwise, \end{cases} \tag{9}$$

where $\lambda$ is a random number.

The controller plays a vital role in the coordinated control system and is an important link to achieve the control goal. To overcome the issue of slow response and poor ability of online tuning of traditional controllers, an improved seagull optimization algorithm (ISOA) is used to optimize the parameters of the PI controller of the energy storage; $k_p$ (scale coefficient) and $k_i$ (integration time coefficient). ISOA can identify the global optimal values of $k_p$ and $k_i$ as per the control principle shown in Figure 4.

**TABLE 2 Hybrid energy storage capacity configuration.**

| Type | Parameter | Value |
|---|---|---|
| Battery | Rated power (kW) | 300 |
| | Capacity (kWh) | 750 |
| | Initial *SOC* (%) | 65 |
| | Depth of discharge (%) | 20 ~ 90 |
| Supercapacitors | Rated power (kW) | 100 |
| | Capacity (kWh) | 10 |
| | Initial *SOC* (%) | 65 |
| | Depth of discharge (%) | 20 ~ 90 |

In Figure 4, Y (t) is the actual input quantity; U (t) is the reference quantity; $e_1$ and $e_2$ are the deviation values; and $e_{c1}$ and $e_{c2}$ are the deviation change rates.

The time integration performance index of the absolute value of the error e (t) is used as the minimum objective function for parameter selection (Li et al., 2021a). The input squared term is added to the objective function to avoid excessive control, as given by Eq. 10.

$$F = \int_0^\infty \left(\omega_1 |e(t)| + \omega_2 U^2(t)\right) dt, \tag{10}$$

where $\omega_1$ and $\omega_2$ are the weight coefficients; usually, $\omega_1$ is set to 0.999 and $\omega_2$ is set to 0.001.

At the same time, the overshoot is used as one of the optimal objective functions to avoid overshooting (Yang et al., 2021b), and the objective function can be represented using Eq. 11.

$$J(t) = J(t) + 100|e(t)| \;\; if\, e(t) < 0. \tag{11}$$

# 5 Simulation analysis

## 5.1 Power fluctuations are flattened

The effectiveness of the proposed strategy is verified using historical measured data of a 750 kW distributed photovoltaic system (Li et al., 2023c). A simulation model with a sampling interval of 1 min is built in MATLAB based on the topology shown

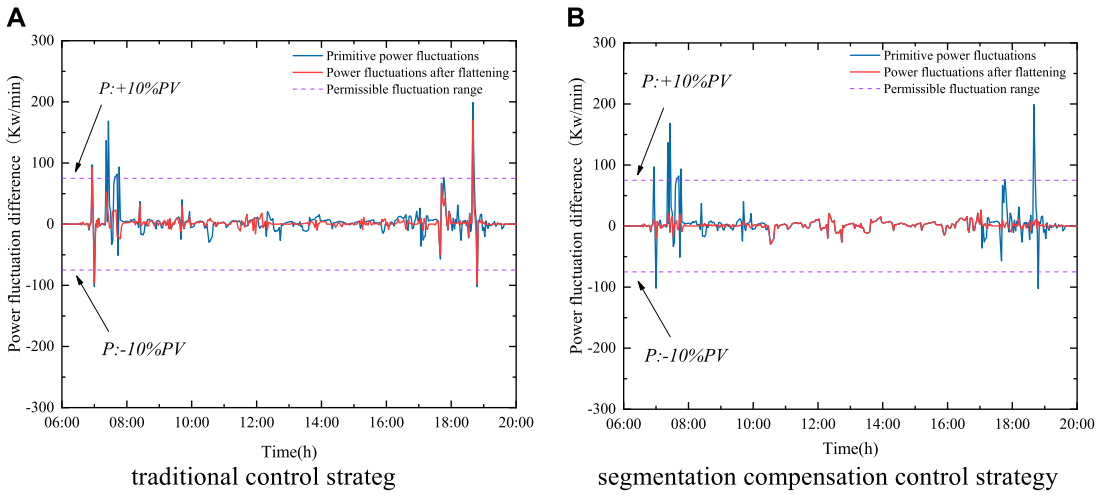


FIGURE 5
Comparison of the power fluctuation flattening effect on typical sunny days. **(A)** Traditional control strategy. **(B)** Segmentation compensation control strategy.

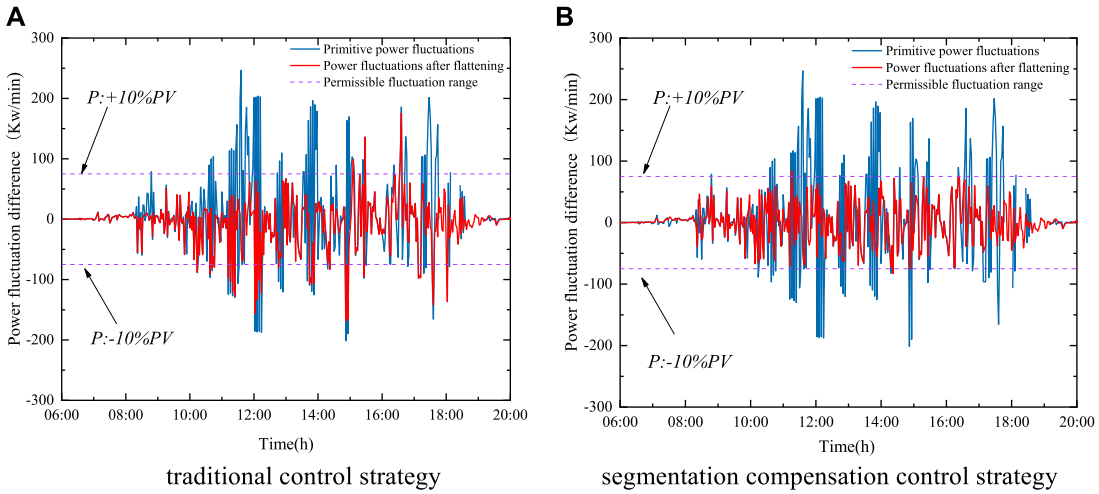


FIGURE 6
Comparison of the power fluctuation flattening effect in typical multi-cloud scenarios. **(A)** Traditional control strategy. **(B)** Segmentation compensation control strategy.

in Figure 1. Two sets of output power data in typical sunny and cloudy weather were used to analyze the flyer battery control strategy and the hybrid energy storage segmentation compensation strategy, respectively. The hybrid energy storage capacity configuration is shown in Table 2.

Figures 5, 6 show comparisons of the power fluctuation flattening effect for the traditional and proposed control strategies during sunny and cloudy days, respectively. Within the period 8:00 ~ 19:00, the generated power of the distributed photovoltaic system fluctuates due to environmental and external conditions. When the traditional control strategy of a single battery is used to mitigate power fluctuations, the response is slow due to the large energy density of the battery. Thus, the battery is not a good candidate to mitigate short-term fluctuations in sunny weather scenarios (Figure 5A). At the same time, due to the maximum discharge power of the battery and capacity limitations, though the positive power fluctuations can be effectively suppressed in multi-cloudy weather scenarios, some negative power fluctuations cannot be effectively suppressed, as shown in Figure 6A. As shown in Figures 5B, 6B, when the strategy proposed in this paper is used to flatten the power fluctuation, the wavelet packet algorithm decomposes the power to identify the working condition of the hybrid storage system. The hybrid energy storage device does not work when the power fluctuation is within the permissible fluctuation range, while it is activated when power fluctuation exceeds this range. The hybrid energy storage device coordinates and cooperates to reasonably

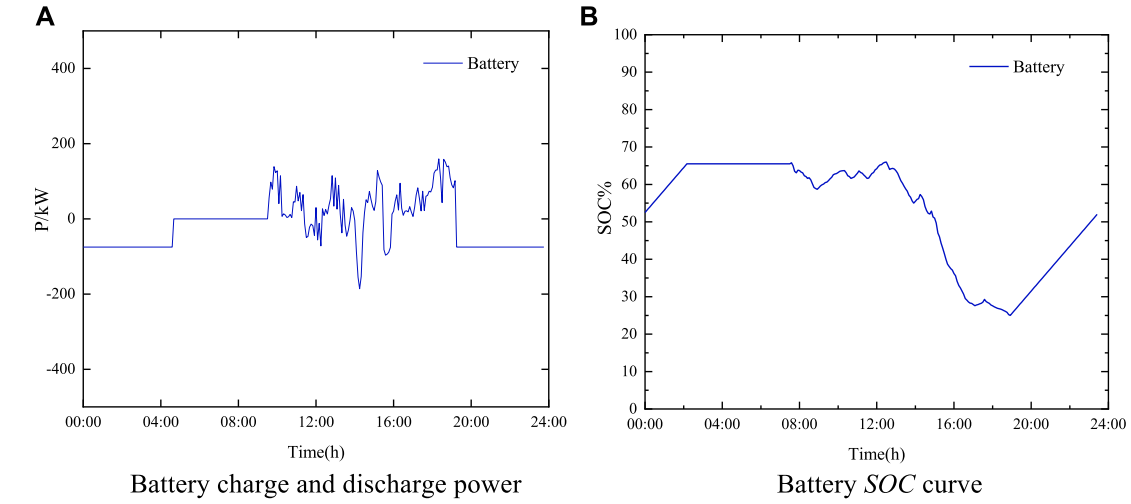


FIGURE 7
Single battery under the traditional control strategy. **(A)** Battery charge and discharge power. **(B)** Battery *SOC* curve.

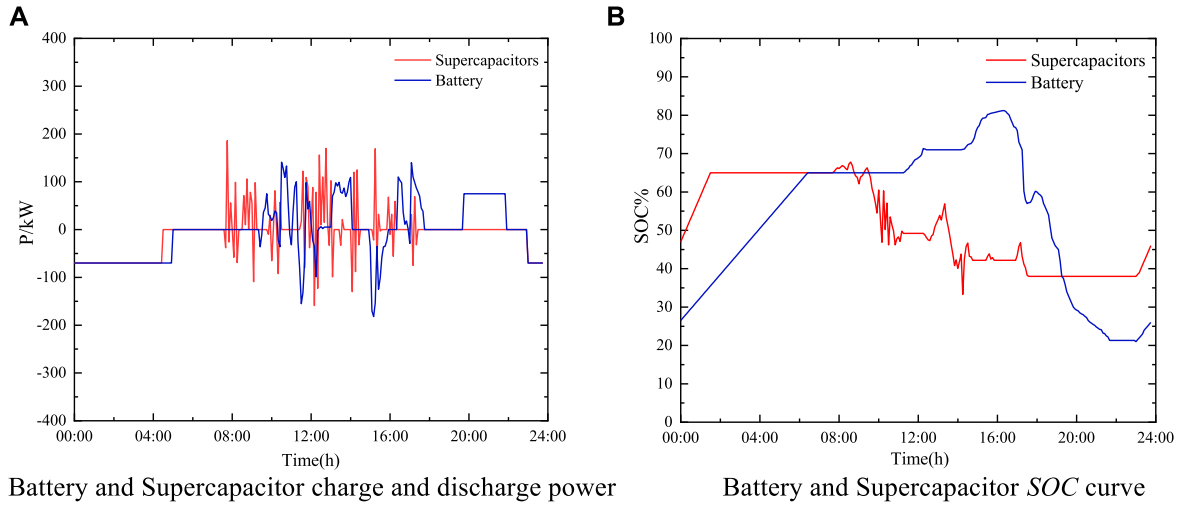


FIGURE 8
Hybrid energy storage under the proposed control strategy. **(A)** Battery and supercapacitor charge and discharge power. **(B)** Battery and supercapacitor *SOC* curve.

reduce the number of battery charges and discharges, and the supercapacitor responds quickly to short-term fluctuations. As can be seen from the two figures, most of the power fluctuations can be suppressed within the allowable fluctuation range.

In order to further verify the effectiveness of the battery charge and discharge control method proposed in this paper, the charging and discharging power and *SOC* modes are analyzed.

Figure 7 shows the battery output power profile and *SOC* curve under the traditional control strategy. In this strategy, the required compensation power is borne by the battery. The continuous changes in battery *SOC* may cause serious damage to the battery and reduce its operating life.

Figure 8 shows the power profile and *SOC* curve under the strategic hybrid energy storage device proposed in this paper. Within the duration of 8:00~19:00, the supercapacitor and the battery cooperate to quickly mitigate high-frequency power fluctuations, while the battery continues to compensate for low-frequency power fluctuations. This strategy reduces the frequency of battery charging and discharging and improves the service life of the device. Between 15:30 and 16:00, the battery *SOC* is higher than the overcharge threshold limit. As such, the control strategy acts to slow down the charging speed and avoid overcharging. Between 19:00 and 20:00 and during the peak electricity price period, the battery *SOC* violates the over-discharge threshold limit, and the control system acts to slow down the discharge speed until the *SOC* is less than 20%, after which the device is charged during low electricity prices at midnight until the rated *SOC* is reached and the device is shut down.

**TABLE 3 Basic information of test functions.**

| Function name | Expression | Dimension | Search for space | Optimal solution |
|---|---|---|---|---|
| F1 | $f(x) = \sum_{i=1}^{n} x_i^2$ | 60 | [-5.88,5.88] | 0 |
| F2 | $f(x) = \sum_{i=1}^{n} i x_i^4 + \text{Gauss}(0, 1)$ | 30 | [-1.01,1.01] | 0 |
| F3 | $f(x) = \sum_{i=1}^{n} [x_i^2 - 10\cos(2\pi x_i) + 10]$ | 10 | [-5.12,5.12] | 0 |
| F4 | $f(x) = -20^{*}e^{-0.2^{*}\sqrt{\frac{1}{n}\sum_{j=1}^{n} x_j^2}} - e^{\frac{1}{n}\sum_{j=1}^{n}\cos(2\pi x_j)} + 20 + e$ | 60 | [-36,36] | 0 |
| F5 | $f(x) = \frac{1}{1000}\sum_{i=1}^{n} x_i^2 - \prod_{i=1}^{n}\cos(\frac{x_i}{\sqrt{i}}) + 1$ | 120 | [-700,700] | 0 |

**TABLE 4 Comparison of optimization results of standard functions.**

| Function | Algorithm | Optimal value | Average value | Standard deviation | Time |
|---|---|---|---|---|---|
| F1 | ISOA | 1.94E-163 | 3.41E-1.63 | 0 | 0.05323 |
| | SOA | 2.73E-126 | 5.63E-119 | 6.5216E-119 | 0.05467 |
| | WOA | 2.17E-49 | 8.29E-41 | 1.13567E-43 | 0.05527 |
| | PSO | 0.007231 | 0.044327 | 0.026593475 | 0.05677 |
| F2 | ISOA | 27.3803 | 28.85743 | 0.473268 | 0.05471 |
| | SOA | 28.3157 | 29.46878 | 0.68253 | 0.05358 |
| | WOA | 11.8576 | 40.53876 | 33.5217 | 0.05526 |
| | PSO | 1875.468 | 6145.576 | 2,758.643 | 0.05549 |
| F3 | ISOA | 0 | 4.75E-10 | 8.04216E-10 | 0.05419 |
| | SOA | 5.59E-14 | 5.63E-01 | 1.7876324096 | 0.05336 |
| | WOA | 28.5436 | 46.57915 | 10.52548963 | 0.06692 |
| | PSO | 163.5796 | 227.6794 | 28.85457654 | 0.06715 |
| F4 | ISOA | 8.86E-16 | 8.86E-16 | 1.96879E-31 | 0.05237 |
| | SOA | 1.52E-14 | 1.74E-14 | 3.187615E-15 | 0.05368 |
| | WOA | 0.000000765 | 5.75E-2 | 0.268751564 | 0.06725 |
| | PSO | 3.7267 | 4.41579 | 0.386789954 | 0.06949 |
| F5 | ISOA | 0 | 1.51E-10 | 4.96348E-10 | 0.05524 |
| | SOA | 0 | 0.001367 | 0.004568761 | 0.05352 |
| | WOA | 5.64E-13 | 0.005937 | 0.006267545 | 0.06363 |
| | PSO | 0.42678 | 0.621,367 | 0.124156379 | 0.07127 |

## 5.2 Improved seagull optimization algorithm

The proposed ISOA is compared with three algorithms, namely, the ordinary seagull algorithm, particle swarm optimization (PSO) algorithm, and whale optimization algorithm (WOA), to verify its superiority. The simulation parameters are set as follows: population size N = 100, the maximum number of iterations is 200, the initial value of the control factor $f_{ci}$ = 0.8935, and the time constants u and v are set to random numbers between [0, 1] for ISOA. For conventional SOA, the control factor $f_c$ is 1, while the remaining parameters are the same. The parameters of PSO algorithm are as follows: learning factors $c_1 = c_2 = 1.495$ and random numbers $r_1 = r_2 = 0.5$. For WOA, the parameters are convergence factor α = 0.618. The basic information and optimization data of the test function are shown in Tables 3, 4.

**TABLE 5 RMSE and MAE for different algorithms.**

| Algorithm | RMSE | MAE |
|---|---|---|
| ISOA | 1.98E + 00 | 4.1E + 00 |
| SOA | 3.9E + 00 | 4.95E + 00 |
| WOA | 2.1E + 01 | 3.88E + 01 |
| PSO | 6.5E + 02 | 9.88E + 02 |

It can be seen from the data in Table 4 that in terms of solution accuracy, the ISOA optimal value and average value are better than other algorithms for unimodal functions F1 and F2, and for multimodal functions F3, F4, and F5, complexity is increased due to the increase in dimensionality. However, ISOA still has high solution accuracy and reaches the theoretical optimal value, while the solution accuracy of other algorithms is low. In terms of execution time, ISOA is slightly faster than other algorithms, especially in multimodal test functions. The ISOA solution speed is slower than that of SOA because SOA is prone to fall into an early convergence state due to its own optimization mechanism. Hence, the PSO algorithm exhibits immature optimization, thereby reducing the solution time to a certain extent.

In order to test the robustness of ISOA, two evaluation indicators are used: root mean square error (RMSE) and mean absolute error (MAE), based on the average optimal results of each function of different algorithms, and the following Eqs 12, 13 are 1obtained:

$$RMSE = \frac{1}{\sqrt{N}}\sqrt{\sum_{i=1}^{N}(A_i - B_i)^2}, \tag{12}$$

$$MAE = \frac{\sum_{i=1}^{N}|A_i - B_i|}{N}, \tag{13}$$

where $A_i$ is the average of the optimal results generated by the algorithm, $B_i$ is the theoretical optimal value of the corresponding test function, and N is the number of test functions.

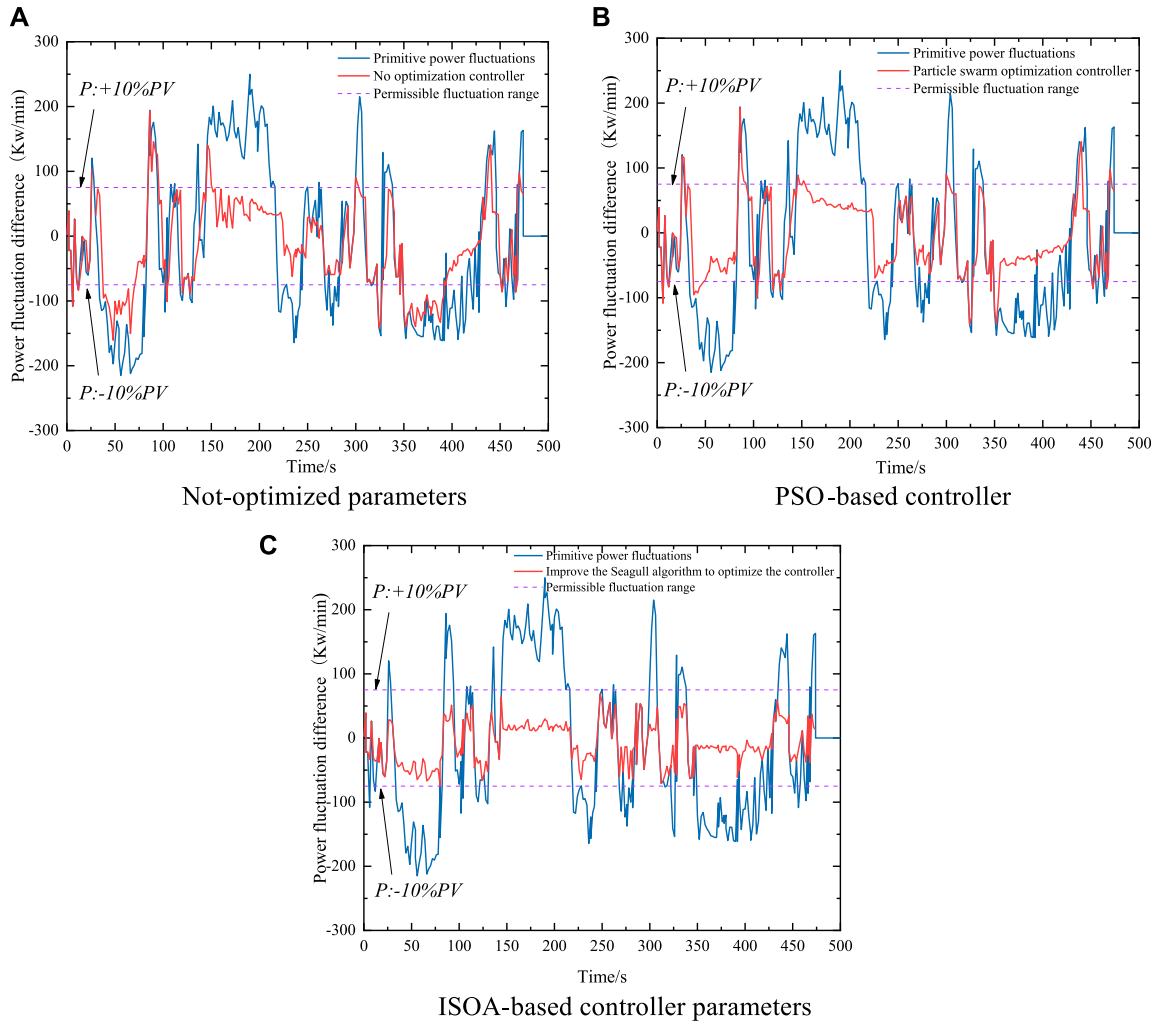


FIGURE 9
Controller simulation comparison. **(A)** Not-optimized parameters. **(B)** PSO-based controller parameters. **(C)** ISOA-based controller parameters.

The RMSE and MAE values of different algorithms are shown in Table 5. It can be observed that the RMSE and MAE of ISOA are the smallest values compared with those of the other three algorithms. This attests that the algorithm proposed in this paper is more robust. In summary, ISOA has good performance in solving unimodal and multimodal reference functions, which shows that the performance of the algorithm is effectively improved by changing the control factor and adding opposing search operators and mutation operations.

In order to further illustrate the ability of the proposed ISOA to mitigate power fluctuation, 500 s with severe fluctuations in multi-cloudy scenarios is investigated. Three sets of comparative experiments, namely, not-optimized controller, PSO-based controller, and ISOA-based controller parameters, are used. As shown in Figure 9.

From the simulation results, it can be seen that the controller optimized by the algorithm proposed in this paper has a short response time, and the control parameters are adjusted online according to power changes. The supercapacitor and battery are controlled to smooth out the power fluctuation in a short time, which, to a certain extent, also makes up for the disadvantages of slow response caused by the large energy density of the battery. The supercapacitor and the battery are fully coordinated, and the power fluctuation is basically flattened within the allowable fluctuation range, indicating that the variable operation strategy adopted in the proposed algorithm can adjust the controller parameters in real time.

## 6 Conclusion

Aiming at the problem of distributed photovoltaic power fluctuation, this paper proposes a segmented compensation strategy for power fluctuation based on the improved seagull algorithm. The controller parameters of the hybrid energy storage system are tuned based on the improved seagull algorithm to smooth out power fluctuation. Simulation results prove the rationality of the proposed strategy.

The segmented compensation strategy of hybrid energy storage proposed in this paper decomposes the original power using the wavelet packet algorithm to realize the initial power distribution within the hybrid energy storage devices and continuously corrects the initial power allocation according to the real-time state of charge. This can not only smoothen the power fluctuations of different amplitudes effectively but also reduce the number of charging and discharging states of energy storage devices, avoid overcharge and discharge phenomena, and extend the service life of the battery. At night, combined with time-of-use electricity price, SOC, and load size, the electricity price difference is used to determine the start and end times of charging and discharging of the device and achieve the optimum economical strategy.

The controller based on the improved seagull algorithm improves the speed of online correction and parameter setting, ensures flexible control of each branch of the hybrid energy storage device, and ensures the accurate implementation of the proposed control strategy.

In the research process of this study, the optimal range of battery residual capacity and capacity configuration in the process of flattening power fluctuations is based on references and past experience, and the multi-functional decoupling capacity configuration research on hybrid energy storage systems can be carried out in the future. At the same time, this paper does not consider the problems that may occur in actual engineering such as differential expansion and control saturation, and in the future, the smooth switching control technology of different working modes of hybrid energy storage systems can be studied from the perspective of actual engineering.

## Data availability statement

The original contributions presented in the study are included in the article/Supplementary Material; further inquiries can be directed to the corresponding authors.

## Author contributions

HC: writing–original draft and writing–review and editing. JC: conceptualization, formal analysis, and writing–review and editing. ZL: writing–original draft and writing–review and editing. AA-S: writing–review and editing. HL: writing–review and editing.

## Funding

This work was supported by the State Key Laboratory of Advanced Electromagnetic Engineering and Technology (Grant No. AEET 2022KF005). The writing of this article has been strongly supported by Curtin University and the State Key Laboratory of Advanced Electromagnetic Engineering and Technology.

## Acknowledgments

The authors would like to express their sincere thanks to Curtin University and the State Key Laboratory of Advanced Electromagnetic Engineering and Technology for their support in writing of this article.

## Conflict of interest

The authors declare that the research was conducted in the absence of any commercial or financial relationships that could be construed as a potential conflict of interest.

## Publisher's note

# References


Chen, C., Yang, X., Lv, H., and Li, Y. (2022). "Optimal configuration of wind turbine hybrid energy storage based on wavelet packet-double fuzzy control," in 2022 25th International Conference on Electrical Machines and Systems (ICEMS) (IEEE), 1–6.

Choi, W., Lee, W., Han, D., and Sarlioglu, B. (2018). New configuration of multifunctional grid-connected inverter to improve both current-based and voltage-based power quality. *IEEE Trans. Industry Appl.* 54 (6), 6374–6382. doi:10.1109/tia.2018.2861737

Fu, W., Jiang, X., Li, B., Tan, C., Chen, B., and Chen, X. (2023). Rolling bearing fault diagnosis based on 2D time-frequency images and data augmentation technique. *Meas. Sci. Technol.* 34 (4), 045005. doi:10.1088/1361-6501/acabdb

Hao, L., Zhenhua, L., Ziyi, C., and Xu, Y. (2022). Insulator fouling monitoring based on acoustic signal and one-dimensional convolutional neural network. *Front. Energy Res.* 10, 906107. doi:10.3389/fenrg.2022.906107

Izci, D., Ekinci, S., and Çetin, H. (2022). "Arithmetic optimization algorithm based controller design for automatic voltage regulator system," in 2022 Innovations in Intelligent Systems and Applications Conference (ASYU) (IEEE), 1–5.

Kawabe, K., and Nanahara, T. (2018). "Integration of dynamic voltage support capability of distributed photovoltaic generation systems for transient stability improvement of power systems," in 2018 IEEE PES Innovative Smart Grid Technologies Conference Europe (ISGT-Europe) (IEEE), 1–6.

Kharrazi, A., Sreeram, V., and Mishra, Y. (2020). Assessment techniques of the impact of grid-tied rooftop photovoltaic generation on the power quality of low voltage distribution network-A review. *Renew. Sustain. Energy Rev.* 120, 109643. doi:10.1016/j.rser.2019.109643

Li, Z., Lan, F., and Zhong, Y. (2022). Measurement-protection-integrated current sensor based on double-bobbin co-winding technology. *High. Volt. Eng.* 48 (11), 4427–4436. doi:10.13336/j.1003-6520.hve.20220537

Li, Z., Cheng, Z., and Chen, X. (2023c). Study on predication method of audible noise valid data for AC transmission lines. *High. Volt. Appar.* 59 (06), 180–187.

Li, Z., Jia, S., Abu-Siada, A., Tong, Y., Zhang, T., and Liu, G. (2023b). Analysis of statistical method and variation characteristic parameters of very fast transient electromagnetic interference. *Energy Rep.* 9, 1304–1314. doi:10.1016/j.egyr.2023.04.135

Li, Z., Jiang, W., Abu-Siada, A., Li, Z., Xu, Y., and Liu, S. (2020). Research on a composite voltage and current measurement device for HVDC networks. *IEEE Trans. Industrial Electron.* 68 (9), 8930–8941. doi:10.1109/tie.2020.3013772

Li, Z., Wu, L., and Xu, Y. (2021c). Risk-averse coordinated operation of a multi-energy microgrid considering voltage/var control and thermal flow: an adaptive stochastic approach. *IEEE Trans. Smart Grid* 12 (5), 3914–3927. doi:10.1109/tsg.2021.3080312

Li, Z., Wu, L., Xu, Y., Wang, L., and Yang, N. (2023a). Distributed tri-layer risk-averse stochastic game approach for energy trading among multi-energy microgrids. *Appl. Energy* 331, 120282. doi:10.1016/j.apenergy.2022.120282

Li, Z., Wu, L., Xu, Y., and Zheng, X. (2021b). Stochastic-weighted robust optimization based bilayer operation of a multi-energy building microgrid considering practical thermal loads and battery degradation. *IEEE Trans. Sustain. Energy* 13 (2), 668–682. doi:10.1109/tste.2021.3126776

Li, Z., Yu, C., Abu-Siada, A., Li, H., Li, Z., Zhang, T., et al. (2021a). An online correction system for electronic voltage transformers. *Int. J. Electr. Power & Energy Syst.* 126, 106611. doi:10.1016/j.ijepes.2020.106611

Maneesh, (2015). "Frequency control of a microgrid by using PI controller," in 2015 International Conference on Energy, Power and Environment: Towards Sustainable Growth (ICEPE) (IEEE), 1–5.

Ming, S. H. E. N., Yafei, C. H. A. N. G., Ren, G. A. O., and Xiangqian, T. O. N. G. (2018). "Control strategy for smoothing the microgrid tie-line power fluctuations based on back-to-back converter," in 2018 IEEE International Power Electronics and Application Conference and Exposition (PEAC) (IEEE), 1–6.

Nan, Y., Di, Y., Zheng, Z., Jiazhan, C., Daojun, C., and Xiaoming, W. (2018). Research on modelling and solution of stochastic SCUC under AC power flow constraints. *IET Generation, Transm. Distribution* 12 (15), 3618–3625. doi:10.1049/iet-gtd.2017.1845

Pinheiro, A. L., Ramos, F. O., Neto, M. M., Lima, R. N., Bezerra, L. G., and Washington, A. (2021). "A review and comparison of smoothing methods for solar photovoltaic power fluctuation using battery energy storage systems," in 2021 IEEE PES Innovative Smart Grid Technologies Conference-Latin America (ISGT Latin America) (IEEE), 1–5.

Shi, K., Li, D., Li, Y., Wu, Y., Yao, L., and Liao, S. (2021). "Optimal scheduling of integrated energy system considering distributed photovoltaic power fluctuation," in 2021 3rd Asia Energy and Electrical Engineering Symposium (AEEES) (IEEE), 932–937.

Technical regulations for connecting photovoltaic power stations to the power grid (2011). *Technical regulations for connecting photovoltaic power stations to the power grid*. Doctoral dissertation.

Weng, L. G., Feng, X. L., Jin, D. J., Ying, H. H., and Yue, S. H. (2023). "A hybrid energy storage system based on wavelet packet decomposition technology for photovoltaic power smoothing," in 2023 International Conference on Power Energy Systems and Applications (ICoPESA) (IEEE), 369–375.

Xie, X., Wang, H., Tian, S., and Liu, Y. (2015). "Optimal capacity configuration of hybrid energy storage for an isolated microgrid based on QPSO algorithm," in 2015 5th International Conference on Electric Utility Deregulation and Restructuring and Power Technologies (DRPT) (IEEE), 2094–2099.

Xu, P., Fu, W., Lu, Q., Zhang, S., Wang, R., and Meng, J. (2023). Stability analysis of hydro-turbine governing system with sloping ceiling tailrace tunnel and upstream surge tank considering nonlinear hydro-turbine characteristics. *Renew. Energy* 210, 556–574. doi:10.1016/j.renene.2023.04.028

Yang, N., Dong, Z., Wu, L., Zhang, L., Shen, X., Chen, D., et al. (2021b). A comprehensive review of security-constrained unit commitment. *J. Mod. Power Syst. Clean Energy* 10 (3), 562–576. doi:10.35833/mpce.2021.000255

Yang, N., Qin, T., Wu, L., Huang, Y., Huang, Y., Zhang, L., et al. (2022b). A multi-agent game based joint planning approach for electricity-gas integrated energy systems considering wind power uncertainty. *Electr. Power Syst. Res.* 204, 107673. doi:10.1016/j.epsr.2021.107673

Yang, N., Yang, C., Wu, L., Shen, X., Jia, J., Li, Z., et al. (2021a). Intelligent data-driven decision-making method for dynamic multisequence: an E-seq2seq-based SCUC expert system. *IEEE Trans. Industrial Inf.* 18 (5), 3126–3137. doi:10.1109/tii.2021.3107406

Yang, N., Yang, C., Ye, D., Jia, J., Chen, D., Shen, X., et al. (2022a). Deep learning based SCUC decision making: an intelligent data driven approach with self learning capabilities. *IET Generation, Transm. Distribution* 16 (4), 629–640. doi:10.1049/gtd2.12315

You, M., Wu, Y., Wang, Y., Xie, X., and Xu, C. (2022). "Parameter optimization of PID controller based on improved sine-SOA algorithm," in 2022 IEEE International Conference on Mechatronics and Automation (ICMA) (IEEE), 12–17.

Zhang, Y., Fu, W., Chen, X., Hu, S., Zhang, L., Xia, Y., et al. (2022). An optimal combining attack strategy against economic dispatch of integrated energy system. *IEEE Trans. Circuits Syst. II Express Briefs* 70 (1), 246–250. doi:10.1109/tcsii.2022.3196931

Zhang, Y., Wei, L., Fu, W., Chen, X., and Hu, S. (2023). Secondary frequency control strategy considering DoS attacks for MTDC system. *Electr. Power Syst. Res.* 214, 108888. doi:10.1016/j.epsr.2022.108888

Zhu, B., Liu, Y., Zhi, S., Wang, K., and Liu, J. (2022). A family of bipolar high step-up zeta–buck–boost converter based on "coat circuit". *IEEE Trans. Power Electron.* 38 (3), 3328–3339. doi:10.1109/tpel.2022.3221781